Characterization of Soil Erosion Indicators Using Hyperspectral Data From a Mediterranean Rainfed Cultivated Region

Thomas Schmid, *Member, IEEE*, Manuel Rodríguez-Rastrero, Paula Escribano, Alicia Palacios-Orueta, Eyal Ben-Dor, Antonio Plaza, *Fellow, IEEE*, Robert Milewski, Margarita Huesca, Ashley Bracken, Víctor Cicuéndez, Marta Pelayo, and Sabine Chabrillat

***Abstract*—The determination of surface soil properties is an important application of remotely sensed hyperspectral imagery. Moreover, different soil properties can be associated with erosion processes, with significant implications for land management and agricultural uses. This study integrates hyperspectral data supported by morphological and physico-chemical ground data to identify and map soil properties that can be used to assess soil erosion and accumulation. These properties characterize different soil horizons that emerge at the surface as a consequence of the intensity of the erosion processes, or the result of accumulation conditions. This study includes: 1) field and laboratory characterization of the main soil types in the study area; 2) identification and definition of indicators of soil erosion and accumulation stages (SEAS); 3) compilation of the site-specific MEDiterranean Soil Erosion Stages (MEDSES) spectral library of soil surface characteristics using field spectroscopy; 4) using hyperspectral airborne data to determine a set of endmembers for different SEAS and introducing these into the support vector machine (SVM) classifier to obtain their spatial distribution; and 5) evaluation of the accuracy of the classification applying a field validation protocol. The study region is located within an agricultural region in Central Spain, representative of Mediterranean agricultural uses dominated by a gently sloping relief, and characterized by soils with contrasting horizons. Results show that the proposed method is successful in mapping different SEAS that indicate preservation, partial loss, or complete loss of fertile soils, as well as down-slope accumulation of different soil materials.**

***Index Terms*—Hyperspectral data, rainfed agriculture, semiarid, soil erosion, support vector machine (SVM).**

Manuscript received September 22, 2014; revised March 28, 2015 and June 26, 2015; accepted July 10, 2015. Date of publication September 10, 2015; date of current version February 09, 2016. This work was supported in part by the National Project (AGL2010-17505) by the Spanish Science R&D program, in part by the European Facility for Airborne Research (EUFAR), and in part by the EnMAP Science Program funded by the German Federal Ministry of Economics and Technology and internal support from GFZ in Potsdam.

T. Schmid, M. Rodríguez-Rastrero, and M. Pelayo are with the Department of Environment, Centro de Investigaciones Energéticas, Medioambientes y Tecnológicas (CIEMAT), 28040 Madrid, Spain (e-mail: thomas.schmid@ciemat.es).

P. Escribano is with the Department of Conservation Biology, Estación Biológica de Doñana, Consejo Superior de Investigaciones científicas (CSIC), 41013 Sevilla, Spain.

A. Palacios-Orueta, M. Huesca, and V. Cicuéndez are with the Departamento de Sistemas y Recursos Naturales, E.T.S.I. Montes, Universidad Politécnica de Madrid (UPM), 28040 Madrid, Spain.

E. Ben-Dor is with the Department of Geography and Human Environment, Tel Aviv University, Tel Aviv 69978, Israel.

A. Plaza is with the Hyperspectral Computing Laboratory, University of Extremadura, E-10071 Cáceres, Spain.

R. Milewski and S. Chabrillat are with German Research Centre for Geosciences (GFZ), 14473 Potsdam, Germany.

A. Bracken is with the Department of Geography, University of Lethbridge, Lethbridge, AB T1K 3M4, Canada.

Color versions of one or more of the figures in this paper are available online at http://ieeexplore.ieee.org.

Digital Object Identifier 10.1109/JSTARS.2015.2462125

I. Introduction

THE ANALYSIS of the data obtained by optical remote sensing techniques such as soil spectroscopy and hyperspectral imagery using hundreds of spectral bands has proven in the past 10 years to be an effective way to characterize and monitor surface soil variables [1], [2] that would allow soil erosion processes to be determined. These techniques use field and airborne sensors, respectively, to provide data for determining surface properties based on the analysis of soil spectra within the visible and near-infrared (VIS and NIR, 400–1000 nm) and short wave infrared (SWIR, 1000–2500 nm) regions. In these spectral regions, inorganic and organic components such as clay minerals, soil organic matter (SOM), iron oxides, or calcium carbonate ($CaCO_3$) interact with the electromagnetic radiation and produce characteristic absorption features in soil reflectance spectra that can be used to identify soil properties when soils are exposed at the surface and vegetation cover is low [3]–[5]. Therefore, soil spectra with these properties are easily obtained within Mediterranean regions where it is common to have large regions of bare soil surfaces [6], [7].

Cultivation and land use practices have a long history within the Mediterranean region exploiting soils as a natural resource. The soils are an essential factor contributing to agricultural production and their inadequate management is endangering their quality and productivity [8]. In these regions, plant cover, land uses, and topography are considered the most important factors affecting the intensity of soil erosion [9], [10]. The consequence of widespread tillage activities contributes to the transformation of soil landscapes within Mediterranean environments [12]. Climatic conditions such as an intense summer drought, largely determine the types of crops that can be cultivated. Cereals, olive trees, and vineyards are considered as typical crop types of the Mediterranean rainfed agriculture [13]. It is common that these types of cultivations have exposed bare soil surfaces throughout the annual cycle. Given that most of the soil erosion in the Mediterranean region is due to rainfall (splash and wash) [11], soils that support these types of cultivations form part of a fragile ecosystem.

Soil erosion in these agricultural environments can only be explained as a combined effect of tillage practices and water erosion processes [14]. In flat cultivated plots, tillage activities for consecutive years cause soil material to be mixed and spread over the terrain. On sloping surfaces, the maximum soil displacement occurs when tillage is carried out in the down-slope direction. Correspondingly, soil that is removed on the upper slopes will accumulate on the lower slopes forming small alluvial fans [9]. Therefore, the plowing activities modify the soil structure and cause a net loss of soil with no visible erosion features, such as rills or gullies [12], [14].

The soil transformation may involve the whole or partial loss of fertile soil or a mixture or inversion of the differentiated layers that constitute the soil, known as soil horizons. This is particularly relevant in the case of soils consisting of horizons with contrasting properties, which have a widespread representation in the study region [12], [15]. Soils that have been eroded as a result of plowing, will expose different surface (A) or subsurface (B and C) horizons [12] with significant differences in their physical and chemical properties, such as color, pH, SOM, texture, structure, consistence, coarse fragments (CF), free iron oxides, $CaCO_3$, and/or clay minerals [15]. These surface soil properties may vary significantly over short distances and are a key factor to be taken into consideration when planning sampling strategies for studying soil erosion [16]. Furthermore, these soil properties can be considered as soil erosion indicators which must be carefully brought into context with the pedological characteristics found in the study region. A spatial distribution of surface soil properties can be carried out by obtaining soil surface data from reference plots using field, airborne, and/or satellite-borne sensors with different spectral and spatial resolutions using spectroradiometer, hyperspectral, and multispectral data, respectively [17], [18]. In this case, the region of interest will depend on the scene size of the airborne or satellite-borne sensor. This approach is also applied to soil erosion studies using sensors with different spatial, spectral, and temporal resolutions [19], [20]. Further studies, within the Mediterranean region, analyzed data from a combination of sensors at different spatial and spectral resolutions to extrapolate specific soil information obtained from the field plot to a wider region using hyperspectral and/or multispectral sensors, respectively [21]–[23]. In these studies, the compilation of soil spectral libraries with measurements taken in the field and/or in the laboratory serves as a spectral reference of soil properties and compositions that can be used to compare and validate spectral information obtained from any hyperspectral sensor. Therefore, the reference spectra can be used to characterize soil parameters and map the validation of the spatial distribution of surface soil properties when hyperspectral imagery is available and soils were exposed at the surface [2], [6], [7].

The main objective of this work is to develop an integrated method that uses high-resolution remote sensing data together with morphological and physico-chemical field and laboratory data, to identify and characterize different soil properties on the surface that can be used as indicators of tillage-induced soil erosion. A gently sloping agricultural region within Central Spain was selected as representative of Mediterranean agricultural uses with an important presence of soils with contrasting horizons.

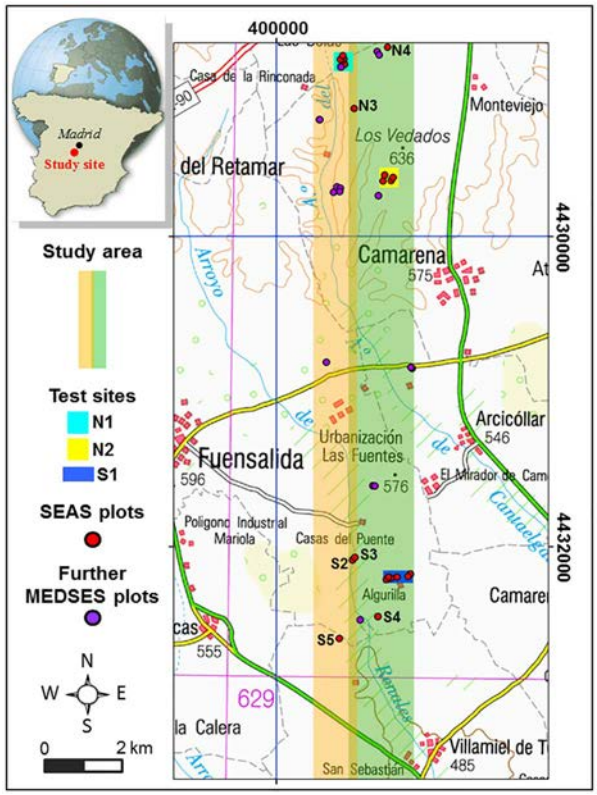

Fig. 1. Camarena study region with two hyperspectral flight lines acquired during the 2011 EUFAR campaign.

Specific objectives include: 1) improving the pedological knowledge of the region through field and laboratory characterization of the main soil types; 2) identifying and defining the corresponding indicators of soil erosion and accumulation stages (SEAS) in terms of the presence of different soil horizons at the surface; 3) compiling a site-specific spectral library of the soil surface characteristics related to erosion using field spectroscopy; 4) using hyperspectral airborne data to extract a set of endmembers for the different SEAS that are used for training the support vector machine (SVM) classifier and obtaining a spatial distribution of the individual classes representing the different stages; and 5) estimating the accuracy of the classification using field validation points and a confusion matrix.

The proposed integrated method provides a qualitative assessment of surface soil erosion and accumulation. The potential use of the methodology is based on the different soil horizons emerging at the surface that has contrasting properties. The identification of these properties is important to determine environmental and agricultural implications that may influence conditions of current and possible future land uses [24], [25].

II. Description of the Study Region

The study region (see Fig. 1), with an area of 49 km^2, is located within the north-western part of the autonomous community of Castilla-La Mancha in the Province of Toledo approximately 50 km SW from Madrid. The relief is undulating with gentle slopes with a decreasing elevation from north to

south of 650 m above mean sea level (a.m.s.l.) to 500 m a.m.s.l., respectively.

The climate is Mediterranean with a continental character, where the average monthly temperature ranges from 6.1 to 24.7 °C and the monthly rainfall varies from a minimum of 7 mm (July) to a maximum of 56 mm (November) with an average yearly rainfall of 429 mm [26]. The lithological substrate is mainly formed of Miocene arkoses and marls and Quaternary sediments [27]. Coarse and medium arkoses, with no significant presence of $CaCO_3$, dominate in the northern part of the study region; where *Haploxeralfs* and *Haploxerepts* (A/Bt/C or A/Bw/C profiles) are the most representative soils [28]. The presence of fine-textured and calcite-rich parent materials (carbonated fine arkoses and lutites), alternating with thin limestone levels, emerge largely in the southern third of the study region. On these latter parent materials, *Calcixerepts* (A/Bw/Ck profiles) constitute the most representative soils [28].

Soil types listed above mainly support agricultural uses such as rainfed cereal crops and vineyards, both occupying about 80% of the total agricultural surface of the study region. The remaining agricultural surfaces consist of olive groves and pastures. Due to traditional methods of soil management, large soil surfaces remain covered by dry crop residue during several months. Dry vegetation coverage is even more widespread as a result of keeping certain fields in fallow for at least 1–2 years before being cultivated again. Soil parameters differ notably between soils from the north and south of the study region. A general comparison shows that soils in the north have higher iron oxide contents (frequent reddish colors), acid, or neutral pH; coarse textures, higher abundance in CF, and harder consistencies [15]. Soils in the south have significant amounts of calcium carbonate and have in generally a basic pH. As is common in Mediterranean agricultural soils, the SOM values are low in the whole study region [15]. This lack of SOM is one of the main reasons that favor erosion and transformation of soils from one place to another [15]. Somewhat higher SOM contents (1.5%–2%) are found in the accumulation stage in toeslopes and terraces.

III. Materials and Methods

A. Field, Airborne, and Cartographic Data Available

Data from field surveys, an airborne campaign, and available ancillary data were used in this study to determine soil erosion indicators (see Fig. 2). This included spectroradiometer data obtained with ASD FieldSpec3 and FieldSpec Pro instruments, covering the spectral range of 350–2500 nm, during selected field campaigns carried out from 2011 to 2014 that were supported by the Spanish National R&D program and the German Research Centre for Geosciences (GFZ) in Potsdam (Germany). Hyperspectral data (airborne aisaEAGLE and aisaHAWK sensors) and Leica ALS50 (II) airborne laser scanner (LIDAR) data were obtained in 2011 by the Natural Environment Research Council (NERC) through a Transnational Access grant from the European Facility for Airborne Research (EUFAR). The 2011 field campaign was realized during the acquisition of the airborne sensor data.

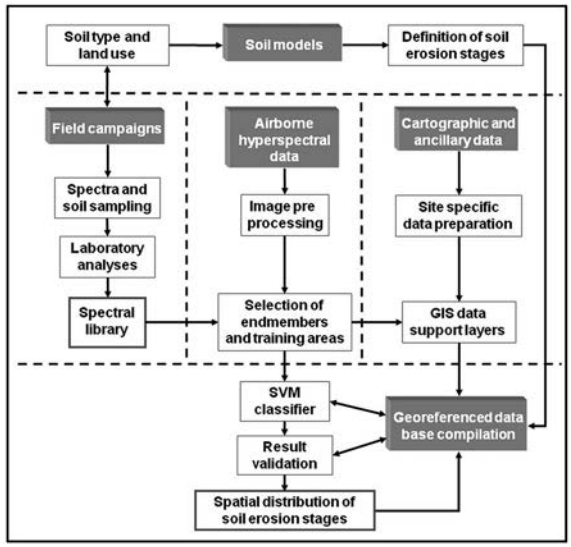

Fig. 2. Method for mapping SEAS.

The purpose of the campaign was to calibrate and validate the hyperspectral data and create a site-specific spectral library.

The aisaEAGLE and aisaHAWK sensors were acquired at an altitude of 5000 m above ground level (a.g.l.) and in tandem over the region on August 8, 2011. The aisaEAGLE is a 12-bit pushbroom sensor with 1024 pixels of swath width [field of view (FOV) $= 39.7°$] across 126 spectral pixels over the range 400–970 nm and a 2.9-nm spectral resolution. The aisaHAWK is a 14-bit pushbroom hyperspectral sensor with 320 pixels of swath width (FOV $= 24.0°$) across 237 spectral pixels over the range 970–2450 nm and a 8-nm spectral resolution. The pixel size at nadir for the aisaEAGLE and aisaHAWK was 3.26 and 6.61 m^2, respectively. A total of six flightlines with an overlap of approximately 30% were acquired. For this study, two flight lines were selected covering an area of 49 km^2, because they included a high proportion of bare soil (approximately 30%) and with the most representative soil types. The Leica ALS50-II LIDAR system was acquired on August 10, 2011 at an altitude of 220 m a.g.l. and was operated with the following specifications: 150 kHz single and multiple pulse in air; max scan rate 90 Hz; FoV 40°–75°; av. 2.5 points/m^2; average point spacing at nadir 0.8 m; XY accuracy 0.1 m; Z accuracy 0.08 m; and swath width 728 m.

Cartographic and ancillary data were obtained mainly from Spanish public institutions (MAGRAMA, IGME, and IGN), which provide topographic and thematic maps, high resolution (0.2 m) orthoimages, and numerical data on their websites [29]–[31]. Furthermore, access to agricultural land use data was also available through the web application Visor SigPac, a geographical information system visualizer [32] with access to relevant cartographic maps and orthoimages.

B. Selection of Indicators for SEAS

An in-depth knowledge of the pedological properties of the region was obtained by means of field observations and analytical characterization of the principal soils. This included studying soil profiles, identifying surface and subsurface horizons,

and obtaining soil samples during the 2011–2013 field campaigns. These data were used to develop site-specific conceptual models of SEAS (Section IV-A) taking into account the soil type, lithology, topography, and land use for defining soil erosion indicators within the study region. The proposed models account for the progressive loss of soil horizons as a consequence of erosion from summits and upper slopes and the accumulation of transported soil material to toe slopes and valley bottoms.

Three sites, with an area of approximately 25 ha each (N1 and N2 in the north and S1 in the south) as well as further test plots (N3, N4 and S2 to S5), were selected within the region where hyperspectral data were acquired (see Fig. 1). These sites contain five and six test plots, respectively. A further eight test plots were selected within the flight lines to complete the representation of the major soil types and related to the agricultural management practices within the study region. The plots represent the different SEAS of well-developed soils formed on arkoses, marls, limestones, and quaternary sediments within a gently sloping topography. During the acquisition of the hyperspectral airborne data in 2011, the test plots were located within fields that had been plowed and in dry conditions.

A primary task was to define and establish the soil erosion indicators according to the soil properties exposed on the surface. The assumption is that increasing tillage-induced soil erosion brings about the progressive removal of soil horizons and the corresponding accumulation of soil materials at the slope bottoms [8]. Therefore, different stages of increasing erosion were identified with emerging A, Bt/Bw, or C/Ck horizons [33] on the soil surface and the corresponding accumulation stage of soil materials down-slope.

The term SEAS is, therefore, qualitative and is based on studies focused on tillage-induced soil erosion [12], [14], [34]. It is defined on the basis of soil morphology criteria, visible primarily under field conditions, as the study region has soils with contrasting horizons and is easily quantifiable in laboratory, in terms of pH, $CaCO_3$ content, free iron oxide content, SOM, or texture.

According to soil physico-chemical properties and morphological characteristics obtained from field work and laboratory analysis, the following indicators of SEAS were selected.

1) Free iron oxides (%): The highest contents of iron oxides are related to Bt horizons in the most evolved soils. Low contents of free iron oxide are present in the A and C horizon. An increase of iron oxides is generally associated with B horizons on the surface [19].
2) Texture: In Alfisols, clay percentage increases from the eluvial A to the Bt horizon, the content is greater in the Bt than in the C horizon, and is normally higher in the C than the A horizon [15]. Moreover, sandy textures are characteristic of footslope accumulation surfaces.
3) $CaCO_3$ (%): As a general character in *Calcixerepts*, the $CaCO_3$ content increases with depth, from the surface A horizon to a calcic Bwk or Ck horizon. High contents of $CaCO_3$ at the surface indicate the consequent loss of the upper A and/or B horizons and the presence of Ck horizons [35]. Frequently, *Haploxeralfs* have small amounts of $CaCO_3$ only in the deeper horizons.
4) SOM (%): The highest values in the study region (1.5%–2%) are associated to accumulation stage in toeslopes and terraces. Values of approximately 1% in the surface layer should be associated with the preservation of the A horizon. Subsurface horizons (Bt and C) commonly show values in a range of 0.1%–0.5% [15].
5) CF (% >2 mm fraction): Generally, when surface erosion is active, the percentage of CF increases at the surface as a consequence of grain-selection [36]. Soils with a high content of limestone and coarse arkose show the highest percentage of CF.
6) pH: Low pH values (<6) are related to surface A horizons in *Haploxeralfs* soils and there is an increase in the pH with soil depth. High pH (>8) values are associated with $CaCO_3$-enriched horizons (Ck).
7) Structure and consistence: Well-defined (strong) blocky structures found at the surface with very hard consistence are typical of Bt horizons in these soils. Hard or moderately hard consistence combined with blocky structure characterize Bw horizons. Weakly defined, platy or massive structures correspond to C horizons [15] in arkose and lutites. Soft or loose consistence is characteristic in sandy deposits of the accumulation stage.
8) Munsell color: Strong chromas and/or reddish hues are associated with free iron oxides, as a field indicator of the presence of B horizons on the surface. White, very light, or pale colors are attributed both to $CaCO_3$-rich horizons as well as sandy-textured accumulation surfaces. Less common darker colors are characterized by moderate SOM contents.

The indicators such as $CaCO_3$, free iron oxides, SOM, and texture can be identified according to specific spectral reflectance characteristics that can be obtained with the soil spectroscopy and hyperspectral imagery [1], [7]. The pH, structure, consistence, and Munsell color have been selected as simple field or laboratory validation criteria.

This knowledge is used as a reference to assess the information that can be obtained with the soil spectroscopy and hyperspectral imagery and is also used for validating the resulting spatial distribution of the erosion and accumulation stages.

C. Field Sampling

Regarding the main objective of the study, an initial constraint of the sampling strategy in this study was the amount of bare soil surface that was exposed during the airborne campaign. This accounted for a surface area of 1383 ha (28.2%) of the total study region. When selecting the different field plots, a preliminary soil survey was based on previous soil and thematic maps and references of the region [14], [27], [32]. Therefore, this preliminary survey compiled soil, lithology, geomorphology, and land use information that was used for selecting regions of interest within the study region. With this information, draft maps of three regions of interest were obtained. A stratified random sampling was carried out for each region by first identifying the different SEAS and then, using a grid of 5×5 m, an area-based sampling with random points

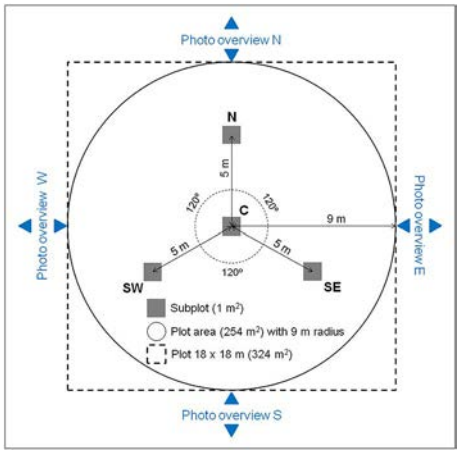

Fig. 3. Field plot area with corresponding subplots.

was generated for each class. A total of 15 field plots were selected within these regions.

The surface cover measurements (soil and vegetation) were taken within selected plots (see Fig. 3). The area occupied by a single plot was related to the spatial resolution of the data acquired [37]. Therefore, taking into account the spatial resolution of the airborne sensor (after preprocessing of sensors, the final spatial resolution is 6 m) and an assumed geometric accuracy of one pixel, the following (1) applies where A is the required plot area (m^2); P is the pixel size (m), and G is the geometric accuracy (pixels)

$$A = (P(1 + 2G))^2. \quad (1)$$

In this case, the area of a plot is $324\ m^2$ which is equivalent to 18×18 m (3×3 pixels). Therefore, the plot design [38] was adapted to carry out the spectral field measurements and obtain soil samples for this study (see Fig. 3). The design has four subplots, each of $1\ m^2$, within an area of $324\ m^2$ which are arranged using a central point C and situating the N, SE, and SW subplots at a distance of 5 m with an angle of 120° between the corresponding subplots. This configuration was easily set up using a survey pole, tape measure, and compass.

During the field campaigns, 12 spectral curves were taken in the four subplots (three in each) for each field plot (using a spectralon white reference). A preprocessing of the spectral curves included the preparation of the individual spectra applying a Savitzky–Golay filter [39] to eliminate irregularities in the spectra carried out with ENVI [40]. Estimation of the spectral homogeneity of the reference endmembers related to the different stages was determined by obtaining the average and standard deviation. Spectral curves that were outside the limit of ± two standard deviations were eliminated and labeled as outliers and removed from further processing.

In each subplot, 500 g of surface soil (the top 1–10 cm depending on soil surface structure) was collected under dry field conditions (no rainfall occurred since July 13, 2011 and the average relative air humidity was 30% with occasional evidence of soil sealing) and transferred to the laboratory to be air-dried and sieved to 2 mm for further analyses. This included physical and chemical analyses, according to standard laboratory procedures, of the soil properties listed in Part I (pH, $CaCO_3$, SOM, CF, texture, free iron oxides, structure, consistence, and Munsell color) [34], [41]. Furthermore, soil profiles were manually excavated or drilled for the central subplots to determine the SEAS according to the proposed conceptual models.

D. Compilation of a Site-Specific Spectral Library

Within the framework of this study, a site-specific spectral library, known as the MEDiterranean Soil Erosion Stages (MEDSES) database, was compiled with representative surfaces related to the different SEAS. Spectral data of different surface covers were also obtained as reference spectra. They included exposed soils affected by different agricultural practices and vegetation related to the different cultivations.

Cartographic and ancillary data (topography, lithology, geomorphology, land use, and aerial orthoimages of 0.5 m) were obtained and integrated into the MEDSES database. These data were used to assist in the identification of endmembers and in the validation of the final results. A geographic information system (GIS) based on ArcGIS [42] was used to manage and compile a georeferenced database of all the generated data of this work. ArcGIS modules (ArcMap, ArcCatalogue, and ArcToolbox) were used to manage the different layers of georeferenced data and present the final map results.

E. Preprocessing of LIDAR and Hyperspectral Imagery

A high-resolution digital elevation model (DEM) of the study region was created from the acquired airborne LIDAR data. The DEM was used for the preprocessing of the hyperspectral data and formed the basis to derive the digital terrain model (DTM) that was used for differentiating changes in the relief when characterizing the soil erosion stages. The DTM represents the bare ground surface excluding objects such as plants and buildings [43]. The preprocessing steps of the LIDAR data included ground filtering, removal of outlier points, and raster interpolation. Ground filtering the LIDAR point cloud was performed with the open source software Boise Center Aerospace Laboratory LIDAR algorithm (BCAL LiDAR tools), which iteratively identifies ground point lying below a thin plate spline surface interpolated from points with the local minimum height in a 4×4 m grid [44]. Additionally, nonobvious outliers were automatically identified and corrected by assessing the vertical displacement to the median elevation of neighboring points following the idea of [45], which propose a threshold for the upper and lower boundary of 0.05 percentage point of the standard normal distribution calculated with the median and median absolute deviation of the neighboring points as parameters. Nearest neighbor interpolation was used for the rasterization of the processed LIDAR point cloud.

The preprocessing procedure included the following steps: 1) an initial preprocessing of the hyperspectral data was performed by the ARSF Data Analysis Node Remote Sensing Group based at Plymouth Marine Laboratory (PML) and the data were delivered as level 1b format (system corrected and

radiometric calibrated sensor data); 2) a systematic image preprocessing was applied including bad bands removal, destriping, and correction for across and along track illumination with the ENVI software [40] routines; and 3) orthorectification, vertical stripping, and data fusion were carried out with routines developed at the GFZ-Potsdam (Pers. Com. K. Segl). Due to a severe, unsystematic distributed vertical striping in the aisaHAWK images, the use of standard destriping software was not useful. Therefore, the destriping routine used, allowed first an automatic correction of homogeneous stripes identified by a 60% deviation from neighboring columns. Then, the remaining stripes were identified by visual inspection and subsequently corrected with the same destriping routine; a data fusion of the aisaEAGLE and aisaHAWK data was necessary as the two sensors have different spectral ranges (129.20–1328.01 and 1002.30–2465.81 nm) and spatial resolutions (3 and 6 m^2). The data fusion routine provides a single composite image cube by combining the multiple image layers from each data set. For this, the aisaEAGLE data were resampled to the spatial resolution of 6 m of the aisaHAWK sensor from the initial 3 m. Due to the low photoconductivity near the wavelength of 1 μm of both the silicon-based aisaEAGLE CDD detector and the aisaHAWK mercury-cadmium-telluride (MCT) detector, an abrupt change in radiance values was observed in the transition range of the two sensors. To provide seamless spectra, another calibration step is included in the data fusion routine for the image bands 245–269 ($0.98-1.07$ μm) where the algorithm replaces the miscalibrated data with artificially calculated at sensor radiance data. The artificial data are derived from spectral reflectance data consisting of representative field surfaces of the study area transformed to at-sensor radiance (Pers. Com. K. Segl). An atmospheric correction was done with the ATCOR4 program [46] using the DEM and the BRDF correction options; and a final step included a fine geometric correction of the two flightlines. Flightlines 1 and 2 with 26 and 24 ground control points, respectively, were warped with the ENVI Map Registration routine using a second-order polynomial. The corresponding root-mean-square errors of 0.46 and 0.49 pixels were obtained.

F. Selection of Training Sites

Endmembers as training sites were obtained to represent the different SEAS. In this case, image processing was done using ENVI [40] with the following routines and included the minimum noise fraction (MNF) where the inherent dimensionality of the data was determined and components with eigenvalues greater than 1 were selected [47]. The corresponding 29 components were input to the pixel purity index (PPI) endmember selection procedure [48] using 50 000 iterations and a threshold of 2.5 to determine spectrally the most pure pixels within the data set. The MNF and PPI results were then projected into an n-dimensional visualizer [49] to determine image-derived endmembers. An initial set of endmembers representing the different soil erosion indicators as well as related land use surfaces was obtained. The selected image-derived endmembers were then compared to the field spectral curves contained in the spectral library using the ENVI Spectral Analyst routine [40] where the spectral angle mapper (SAM) and spectral feature fitting (SFF) techniques were selected. A score of 0–1 was generated for both SAM and SFF via this matching procedure, where the highest score indicates the closest match between the compared spectra. Therefore, the highest score spectral match was analyzed together with its geographic and topographic location, based on the information obtained from the field surveys, the high spatial resolution DTM and the aerial orthoimages, to determine if the endmember was valid. The endmember selection was completed after a two standard deviation was applied to the set of endmembers for each SEAS. Endmembers were considered outliers and were eliminated when any part of their spectra was out of the limits of two standard deviation of the corresponding set of endmembers. Fulfilling these criteria, a final set of image-derived endmembers was obtained for the different stages.

G. Mapping of SEAS Using Hyperspectral Airborne Data and Validation

The supervised SVM classifier [50] was used to categorize the soil surface covers related to the soil erosion and accumulation indicators into several classes according to the spectral pattern of the pixels. In this case, the SVM is a standard classifier that was considered the best option when the amount of training data is limited [51]. The SVM classifier achieves good results even with small training data sets in high-dimensional feature spaces [52]. It was decided to use pure pixels as training data for the SVM in order to increase the confidence of the classifier, as it is well-known that using mixed pixels (not available in labeled form in our context) can also greatly assist for classification purposes [53]. In this case, the SVM classifier was carried out with the Misc Functions of the Department of Statistics (e1071) package [54] as well as using the Geographic Data Analysis and Modeling (raster) [55] and Bindings for the Geospatial Data Abstraction Library (rgdal) [56] packages managed with the R interface [57]. A data set with hyperspectral bands, albedo data, and selected indices was prepared. A continuum removed procedure was applied to the fusioned aisaEAGLE and aisaHAWK image in the VIS (448.9-721.1 nm), NIR (771.8-1324.0 nm) and SWIR (1500.7-1771.9 and 2062.1–2396.4 nm) ranges. The albedo was calculated independently for the different spectral ranges as Albedo $= \sqrt{\sum \mathrm{bi}^2}$ where bi is the band at the ith wavelength. The cellulose absorption index (CAI) and soil related spectral indices such as the clay index (spectral region 2209, 2033, and 2225 nm) and iron absorption depth (spectral region 450–630 nm) were calculated using the HYperspectral SOil MApper (HYSOMA) software [59]. The continuum removed spectral bands together with the CAI, clay index, iron absorption depth, and albedo bands were stacked and a normalization of the 363 bands was obtained as input for the SVM classification. The advantage of scaling to a range of 0–1 is to avoid attributes in greater numeric ranges dominating those in smaller numeric ranges, thus biasing the results [60]. The endmembers that were selected as training sites were used in the SVM classifier applying the Gaussian Radial Basis Function (RBF) kernel in combination with a grid search for the optimization of the penalty C and γ parameters [60]. Applying a 10-fold

cross-validation on the training data, a C of 128 and a γ of $3.051758\mathrm{e}^{-5}$ were determined.

The results were validated using a confusion matrix to obtain the overall accuracies, estimation of the kappa coefficient, individual class accuracies as well as producer and user accuracy [61]. A separate set of ground truth sites were used to assess the confidence limit with which the classification was made. These sites were selected according to the aerial orthoimages of the region and verified in the field obtaining soil profile samples using a gouge auger of the type Purckhauer soil extractor. At each point, the gouge auger was introduced into the plowed soil to a depth of around 90–100 cm. The extracted soil profile was sampled every 10 cm and the samples were brought to the laboratory for further interpretation applying the proposed validation criteria (Section IV-E) for interpreting surface soil conditions and features. A total of 217 validation sites were obtained for all the classes. Where possible, the validation sites were chosen with the same dimension as the field plots (3×3 pixels).

IV. Results and Discussions

A. Defining SEAS for Hyperspectral Remote Sensing

The soils in the study region show contrasting horizons, in terms of their physical and chemical properties, which was a key condition for using techniques such as soil spectroscopy and hyperspectral imagery. This made it possible to differentiate the soil characteristics affected by erosion processes. For this purpose, the properties of the main soils present in the study region were determined through field and laboratory work and used for establishing the soil models (see Fig. 4) that represent the northern and southern region.

The resulting models are based on previous work [15] and the current field surveys, which show that *Haploxeralfs* soils are widely distributed in the northern part of the study region and are sparse in the southern part, whereas the *Calcixerepts* soils are mainly represented in the southern part [19]. Furthermore, the models are based on two assumptions: 1) erosion processes cause underlying horizons to emerge at the ground surface displaying different soil properties that can be used as soil erosion indicators and 2) down-slope accumulation of the eroded soil materials generates deposits with characteristic properties (sandy materials and clays with SOM) at the lowest part of the slope. This is confirmed in the northern (N1) and southern (S1) test-sites and remaining field points where erosion and accumulation sequences have been identified at the surface due to the exposed soil properties of the different horizons that constitute *Haploxeralfs*, *Haploxerepts*, or *Calcixerepts* types of soil, respectively. Therefore, the main horizons present in the study region include A horizons with a low or moderate SOM content; fine-textured B horizons and C (arkosic) or Ck (high $CaCO_3$ content) horizons. As a result, the presence of surfaces with properties related to A, Bt/Bw, or C/Ck horizons was used to define the different SEAS.

The defined SEAS (see Table I) are the basis for the application of imaging spectroscopy techniques, so that the individual stages can be associated with spectral features (Section IV-B).

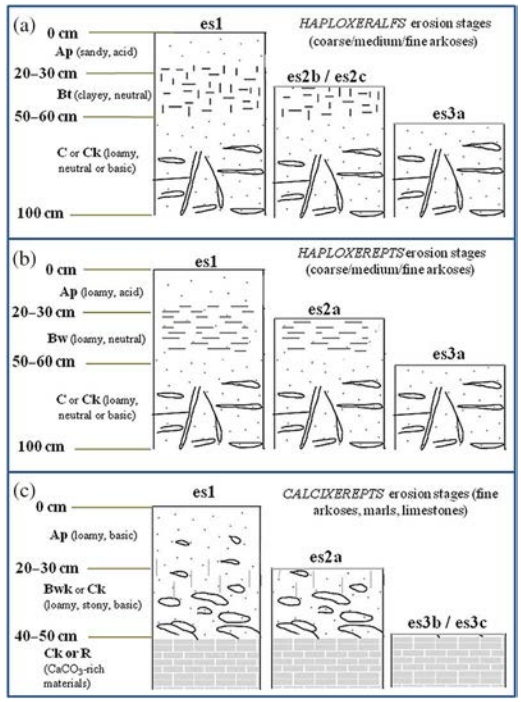

Fig. 4. Conceptual models of soil erosion stages of (a) *Haploxeralfs* and (b) *Haploxerepts* soils in the northern and (c) *Calcixerepts* soils in the southern regions.

The results obtained from the physico-chemical and morphological analyses (see Table II) are as follows.

The accumulation stages (am1 and am2) are defined by sandy (am1) and clayey (am2) textures in the surface layer and often throughout the whole profile. In am1 stage, sand content is generally over 80%, with pale colors, weak structure, and soft consistence [41]. The am2 stage has sand contents lower than 50%, dark colors (associated with moderate content in SOM), and hard consistence as a consequence of the abundant clay.

Slightly eroded soils are represented by the es1 erosion stage, where the soil surface is characterized by low pH and becomes less acid with increasing depth, absence of carbonate, relatively high content of SOM in the surface layer, slight increase in CF with depth, and an important increase of clay content in the middle of the soil profile, which has reddish colors (5YR), an angular structure with a strong grade of development and hard or very hard consistence. All these parameters are related with soils in which the A/Bt/C sequence of horizons is preserved.

Moderately eroded soils are represented in the es2 stage, which is further subdivided into three different stages (es2a, es2b, and es2c). The es2a stage includes soils with an eroded A horizon and a B cambic horizon exposed at the surface. This horizon is characterized by a slightly alkaline pH, presence of $CaCO_3$, moderate clay percentage, grayish-brown colors, moderately developed structure, and hard or moderately hard consistence. Such features are either moderately or slightly different to the parent material (arkose and marl), making it difficult to distinguish B cambic horizons from the C horizons (es3a and es3b stages) exposed at the surface, especially when these surfaces have been plowed.

TABLE I
DESCRIPTION OF SEAS REPRESENTED BY SELECTED FIELD PLOTS

SEAS		Surface description	Code	Field plots
Accumulation stage: deposits in footslope/toeslope positions		Sandy deposits	am1	N1.1, N1.4, N2.2, S1.4
		Clayey and organic matter-rich deposits	am2	S2, S3
Erosion stages	Stage 1: slightly eroded soil. Presence of A horizon	A horizon with subsequent B and/or C horizons	es1	N1.3
	Stage 2: moderately eroded soil. Loss of A horizon, presence of subsurface B horizon	B horizon weathered (*cambic*)	es2a	S1.3
		B horizon with clay accumulation (*argillic*, brown colours)	es2b	N2.1, N2.3
		B horizon with clay and Fe_2O_3 accumulation (*argillic,* reddish colours)	es2c	N1.2, S1.1
	Stage 3: strongly eroded soil. Loss of A and B horizons. Outcropping of C horizons (soil parent material)	C horizon (arkose)	es3a	N3, N4
		Ck horizon (*calcic*, marls)	es3b	S1.6, S4
		Ck horizon; (*calcic)*, R (limestone),	es3c	S1.2, S5

TABLE II
AVERAGE PHYSICO-CHEMICAL AND MORPHOLOGICAL VALUES FOR THE SEAS

SEAS	Depth (cm)	pH	$CaCO_3$ (%)	SOM (%)	Fe_2O_3 (%)	CF (%)	Clay (%)	Sand (%)	Munsell Color*	Structure* (type / grade)**	Consistence* (Rupture resistence)**
am1	0–10	5.5	0.0	0.3	0.14	8	9	83	10YR 7/3	sbk / 1	SH
	20–30	5.8	0.0	0.2	0.13	9	16	77	10YR	sbk / 1	SO-L
	50–60	5.9	0.0	0.2	0.22	9	28	56	10YR 6/3	sbk / 3	MH
am2	0–10	7.6	4.0	1.8	0.27	3	39	35	10YR	abk / 2	HA
	20–30	8.0	5.7	1.9	0.28	2	36	46	10YR 5/2	abk / 1	HA-VH
	50–60	8.4	6.1	2.0	0.28	2	35	42	10YR 5/2	abk-pl / 1	HA-MH
es1	0–10	5.5	0.0	0.7	0.31	10	31	58	10YR 5/3	abk / 3	HA
	20–30	6.0	0.0	0.5	0.60	7	57	40	5YR 4/6	abk / 3	HA-VH
	50–60	6.4	0.0	0.2	0.20	7	45	54	7.5YR	abk / 2	HA-VH
es2a	0–10	7.8	0.0	0.6	0.17	16	22	70	10YR 5/2	sbk / 2	HA
	20–30	8.0	3.9	0.6	0.03	11	27	72	10YR 5/2	abk / 2	MH
	50–60	8.1	0.3	0.2	0.19	9	30	58	10YR 5/3	abk / 3	HA
es2b	0–10	5.7	0.0	0.7	0.45	13	28	59	10YR 5/3	abk / 2	MH
	20–30	6.0	0.0	0.7	0.43	16	33	54	10YR	abk / 2-3	HA
	50–60	6.4	0.0	0.3	0.55	14	47	39	10YR	abk / 3	HA
es2c	0–10	6.9	0.5	0.8	0.55	5	38	51	5YR 4/5	abk / 3	HA
	20–30	6.5	2.3	0.7	0.30	5	47	49	7.5YR	abk / 3	HA-VH
	50–60	6.6	0.0	0.1	0.25	14	31	66	7.5YR	sbk / 2	MH
es3a	0–10	6.1	0.0	0.3	0.27	13	23	69	10YR 4/3	abk / 1	SH-MH
	20–30	5.9	0.0	0.2	0.37	19	25	68	10YR 5/4	abk / 1	HA
	50–60	6.2	0.0	0.2	0.40	17	17	74	7.5YR	m / 0	HA
es3b	0–10	8.2	26.3	1.0	0.25	6	40	38	10YR 6/3	abk / 2	MH
	20–30	8.1	17.3	0.5	0.03	41	29	42	10YR 7/2	pl / 2	SH
	50–60	8.9	10.0	0.4	0.23	3	24	44	10YR 7/2	pl / 1-2	SH
es3c	0–10	8.1	42.8	1.0	0.13	41	30	53	2.5Y 7/2	abk / 1	MH
	20–30	8.0	71.1	0.8	0.01	68	25	59	10YR 8/1	pl / 2	HA
	30–40	8.6	61.2	0.2	0.02	27	28	44	10YR 8/1	pl / 1-2	MH

*Most frequent data observed.
**Type of structure: abk (angular blocky); sbk (subangular blocky); pl (platy); or m (massive). Grade of structure: 0 (structureless); 1 (weak); 2 (moderate); or 3 (strong). Consistence (rupture resistance for dry conditions): L (loose); SO (soft); SH (slightly hard); MH (moderately hard); HA (hard); or VH (very hard) [47].

Erosion stages es2b and es2c represent the outcrop of the Bt horizon in *Haploxeralf*s. The properties of the es2b stage have: low pH and fine textures (moderately high clay content); brown colors and moderately developed angular structures. Those of es2c stage have: low pH, high clay content, redder colors (hue 7.5YR or 5YR), strong angular structures, and hard consistence.

Strongly eroded soils are represented by the es3 erosion stage, in which the entire solum (A and B horizons) has been

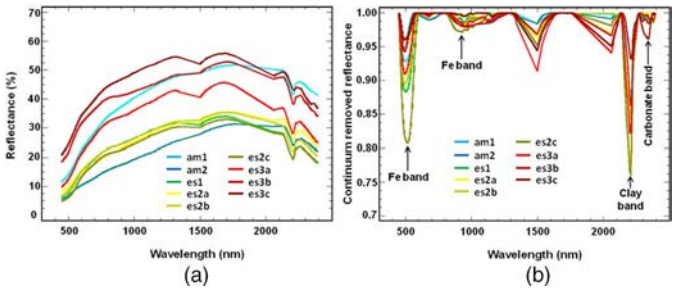

Fig. 5. Mean field spectra of the different SEAS presented as (a) reflectance spectra and (b) with the continuum removed reflectance.

completely removed by erosion. Again, the stage is subdivided according to the type of parent material: arkose (es3a), marl (es3b), and limestone (es3c). Surface covers with an arkose outcrop have: slightly low pH, lack of carbonates, relatively low values of CF, moderately high sand percentage, brown colors, and angular or massive structures with a hard consistence. Those with a marl outcrop have: an alkaline pH with a moderate amount of $CaCO_3$, variable percentages of CF, low sand proportion, light gray colors, trend to platy structures, and weak consistence. Those with a limestone outcrop have: an alkaline pH with a very high proportion of $CaCO_3$, high content in CF and light gray or even white colors, and weak angular blocky to platy structure and hard consistence that characterize these soil landscapes.

B. Compilation of a Site-Specific Spectral Library

The site-specific MEDSES spectral library was compiled with field reference spectra from a total of 36 field plots representing the different SEAS. The library not only contains soil spectra but also covers the surface related to agricultural practices and different rainfed cultivations as follows: fields in fallow (often covered with the remains of dry vegetation from the past cultivation), cereal fields, vineyards, and olive groves. In total, the MEDSES library contains 580 spectra and forms part of a georeferenced database with metadata of the spectra as well as the related field observations and the laboratory soil analyses obtained in this study.

The spectral variation within a field plot was accounted for by obtaining the spectra from the four subplots (three spectra from each subplot). Individual SEAS can be represented by a mean field spectra that were obtained from the spectral curves within one standard deviation [see Fig. 5(a)]. A systematic analyses of the continuum removed spectra over the visible to shortwave infrared ($0.35-2.45$ μm) spectral range [see Fig. 5(b)] showed important differences of the diagnostic absorption features such as iron bands (0.5 μm, 0.87 μm and near 1.0 μm), clay minerals (2.2 μm), and $CaCO_3$ (2.35 μm), respectively [2], [4].

The am1 stage and es3b and es3c stages have overall higher reflectance values than the rest of the stages. These stages are dominated by the high $CaCO_3$ content with peak values in the SWIR (1460–1790 nm). The am1 stage has a characteristic sand shape with maximum reflectance values at 1.6 μm and, in general, maintaining this maximum value till 2.12 μm influenced by the high sand content.

TABLE III
SELECTED IMAGE-DERIVED ENDMEMBERS WITH PPI RANGE AND SPECTRAL ANALYSIS FOR THE SEAS

SEAS	Number of endmembers*	PPI**	Spectral analysis***	
			SAM	SFF
am1	13 (15)	59–1972	0.716–0.885	0.871–0.912
am2	12 (12)	52–304	0.663–0.885	0.834–0.883
es1	12 (12)	73–630	0.662–0.869	0.817–0.869
es2a	13 (15)	53–129	0.631–0.801	0.772–0.846
es2b	14 (15)	54–1417	0.622–0.871	0.828–0.894
es2c	13 (15)	53–288	0.716–0.866	0.787–0.892
es3a	12 (14)	53–628	0.769–0.884	0.834–0.912
es3b	12 (14)	65–870	0.706–0.866	0.798–0.882
es3c	12 (13)	53–1926	0.782–0.861	0.796–0.877
npv	13 (16)	71–1115	0.664–0.850	0.813–0.876

*The numbers in brackets present the endmembers before a two standard deviation were applied.
**PPI determining the most spectrally pure pixels.
***Spectral matching techniques with the SAM and SFF determining the score magnitude where higher scores indicate higher confidence.

Erosion stage es2c showed distinct properties such as high iron oxide content that provides reddish colors and high clay content, both resulting in well-defined spectral characteristics. The es3a could be distinguished from es3b and es3c stages because of the absence of $CaCO_3$ and lower clay content. However, in the erosion stages of es1, es2a, and es2b, surface samples can have similar textures and, therefore, making it difficult to clearly differentiate the corresponding spectral characteristics of these stages.

It is well known that soil spectra are the result of overlapping absorption features of different organic and inorganic components, and subtle differences in spectral shape can provide valuable information on the soil properties [62], [63]. This was especially the case with field sites that represent *es3b*, where a moderate $CaCO_3$ content (15.8%) coincides with a high clay content (32%) that makes it difficult to detect the absorption band of $CaCO_3$.

C. Endmember Selection

The final selection of image-derived endmembers for each SEAS varied between 12 and 14 endmembers (see Table III). Furthermore, nonphotosynthetic vegetation (npv) endmember was introduced as there is a significant coverage of dry vegetation residues left after the harvesting of the cereal crops due to the traditional methods of soil management for rainfed crops in Central Spain. This results in the fields being left for a fallow period of at least 1 year. At the time, when the hyperspectral data were acquired, it is estimated that the npv cover of the entire study region can vary between 15% and 25%.

A first step in the endmember selection was based on the PPI results (see Table III) for the individual endmembers. The values varied greatly and the minimum value accepted was not less than 50. The am1 and es3c had the highest PPI values, whereas es2a had overall low values for all the endmembers. Spectral analysis for the potential endmembers showed that both the SAM and SFF scores were high. The highest score

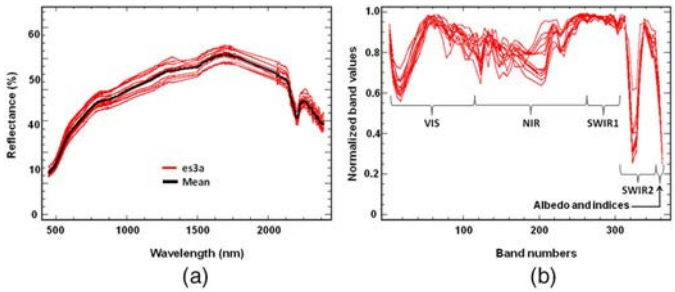

Fig. 6. Example of the soil erosion stage es3a using 12 image-derived endmembers from (a) hyperspectral data and (b) normalized data.

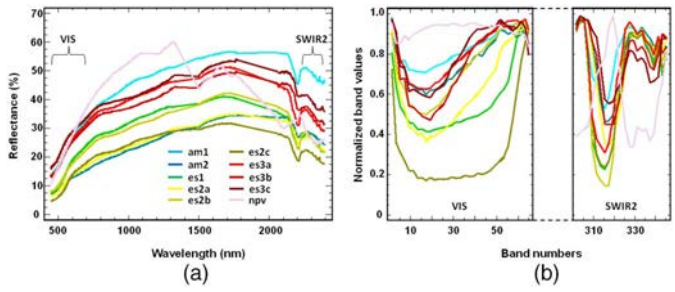

Fig. 7. Mean signatures of SEAS and npv for (a) image-derived endmembers in reflectance values and (b) same endmembers for the VIS and SWIR2 range by using the normalized data.

spectral matches were obtained for the am1 stage and the es3a stage using the SFF technique. The selection of each endmember was confirmed according to the geographic and topographic location, which is based on the information obtained from the field surveys, the high spatial resolution DTM, and the aerial orthoimages. Thereafter, a two standard deviation determined if any endmember had to be eliminated from the corresponding endmember set. In most cases, 1–3 of the endmembers were eliminated for each endmember set representing the different stages and npv.

Each set of endmembers representing the stages was analyzed according to their reflectance values as shown in the example es3a [see Fig. 6(a)]. However, for the further processing of the hyperspectral data set, the data were normalized so that the SVM classifier could be applied. In this case, the corresponding same endmember signatures are shown using the normalized data set [see Fig. 6(b)]. Apart from the optical spectral range, the albedo and indices for each endmember were also included.

The mean values of the image-derived endmembers [see Fig. 7(a)], representing the different SEAS, maintain the main diagnostic spectral features observed in the field spectra (see Fig. 5). The lowest reflectance is maintained by am2 and es2c, where SOM (am2) and high clay content (am2 and es2c) are the main influence. The image-derived es2a reflectance values are somewhat lower than the field values. This is expected as this stage represents a slightly weathered B horizon on arkose material. The soil properties are variable; however, compared to the other stages, es2a has no outstanding soil property that could be spectrally well identified. The mean spectra of es1 and es2b endmembers show spectral similarities and comparing their soil property confirms that the main differences are related to slightly greater iron oxide content for es2b. It has been observed that the es1 endmembers show a high spectral variability compared to es2b. This variability is mainly due to shallow depth of the upper A horizon that is often found as a thin layer covering the B horizon below and is within the influence of the plowing depth. This results in a mixed soil horizon where characteristic soil properties from an original top soil layer become diffuse and may vary considerably from one field to another.

The rest of the SEAS endmembers can be identified according to absorption features and spectral forms that are characteristic of more dominant soil properties such as sandy texture (am1), high clay content and iron content (es2c), high clay content (es3b), and high $CaCO_3$ content (es3c). The npv endmember is well differentiated from the different stages due to the characteristic absorption feature of dry vegetation at 2.09 μm and the high reflectance values within the NIR.

The normalized data for the VIS and SWIR2 ranges [see Fig. 7(b)] show the mean values of the stages and npv well differentiated. The es2c is mostly dominated by the Fe band in the VIS and clay minerals band in the SWIR2. To a lesser extent, this also applies to es1 as well as to further endmembers which have these dominant properties. The $CaCO_3$ absorption feature is well defined for es3c and es3b. The spectral features of npv are also well defined with SWIR2 range.

D. Mapping of SEAS Using Hyperspectral Airborne Data

The spatial distribution of the SEAS (see Fig. 8) represents a unique map related to dominant soil surface properties. The bare soil occupied an area of 1383 ha and the npv of 715 ha, which was a total area of 2098 ha at the time of the data acquisition (see Table IV). This made up 43% of the study region covered by the two hyperspectral flight lines. The remaining 57% of the region was covered by vineyard and olive grove cultivations, riparian vegetation, wood exploitation, and urban surfaces. These regions are subject to change as there are seasonal and annual variations that are influenced by market demand and to a large extent on subsidies available to the farmers. In recent years, there has been a substantial increase in vineyards [29].

The accumulation stage (am1) with 329 ha is the most exposed bare soil surface with a scattered distribution mainly associated with small valley bottoms and footslopes, and more frequently in the northern half of the study region, coinciding with coarser soil textures. The am2 with 226 ha are mainly related to the alluvial surfaces with elevated clay and SOM content. These soils contain the highest content of SOM for the region and are normally cultivated with cereals and allotment plots. The es1, related to well-preserved *Haploxeralfs*, is present in the northern part of the study region occupying 87 ha and virtually absent in the southern part. These surfaces are mainly found on summits and high flat surfaces where erosion processes are minimal. In this case, the soil profile is conserved and an A-horizon is still present, however, under field conditions, it is often difficult to find a succession of soil materials compatible with such soil types. The es2a is the second

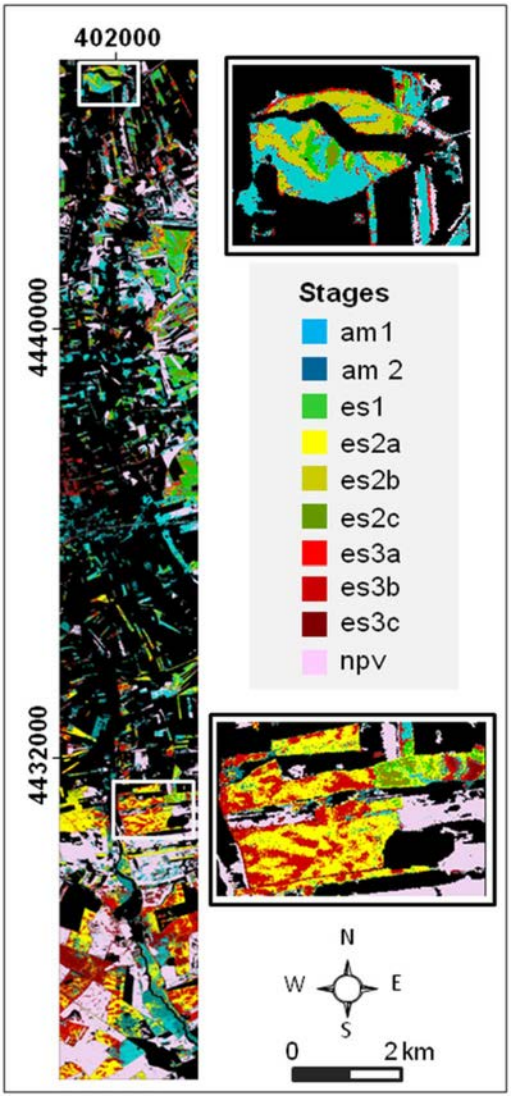

Fig. 8. Distribution of SEAS zones using the SVM classifier.

TABLE IV
AREAS COVERED BY THE DIFFERENT CLASSES

SEAS	Area (ha)	Area (%)	Bare soil and npv (%)	Bare soil (%)
am1	329	6.7	15.7	23.8
am2	226	4.6	10.8	16.4
es1	87	1.8	4.1	6.3
es2a	245	5.0	11.7	17.7
es2b	77	1.6	3.7	5.6
es2c	23	0.5	1.1	1.7
es3a	90	1.8	4.3	6.5
es3b	189	3.9	9.0	13.7
es3c	116	2.4	5.6	8.4
npv	715	14.6	34.1	
Unclassified	2804	57.2		
Total bare soil	1382.6	28.2	65.9	100.0
Total bare soil+npv	2097.7	42.8	100.0	
Total area	4901.9	100.0		

most common bare soil with a total area occupying 245 ha and scattered in the northern half and occupying regions around the classes es2b and es2c. In the southern half, the class is widespread and strongly associated with soils in fine arkoses and marls. In the definition of this erosive stage, it has to be considered that there was a degree of difficulty distinguishing the presence of slightly evolved cambic Bw horizons compared to C horizons from arkoses and marls under the influence of tillage, as both material types have a low competence [48] and are easily arable. Therefore, the main distinguishing feature of Bw and C horizons is the soil structure. As a result of plowing, the alteration of the structure of these horizons hides the differences between the two types of horizons even in carrying out a field validation.

Erosion stages associated with the presence of Bt horizons (es2b and es2c) at the surface occupy small areas (77 and 23 ha). A large percentage of these two stages are found in the northern region due to an increased presence of *Haploxeralfs*.

Stage es3a is characterized by the presence in the surface of C horizons of coarse and medium arkoses (slightly or noncarbonated arkosic materials). The area occupied by this stage (90 ha) is mainly limited to the northern half of the study region, which is closely related to the spatial distribution of these materials. The area occupied by es3b (189 ha) is clearly connected with the prevalence of marls in the southern region. Finally, the es3c erosion stage, corresponding to weathered limestone outcropping, is found in the southern third of the study region (116 ha). This is directly related to the presence of the lithological limestone. The npv is found throughout the study region occupying an area of 715 ha and is considered normal as the region has an important cereal crop production.

Although the different erosion stages have similar spectral characteristics in certain parts of the VIS, NIR and SWIR regions, it was possible to differentiate subtle spectral differences using the SVM classifier and obtain a spatial distribution according to the physico-chemical and morphological characteristics of the soils. Furthermore, topographic characteristics such as slope angle and form affect the final spatial distribution of the different classes of erosion and accumulation.

With reference to the two regions of interest that is selected in Fig. 8, the spatial distribution in the northern region is dominated by the accumulation stage am1. This is due to the deposition of sandy-textured eroded materials, which correspond to the dominating coarse textures of soils within this region. The am2 stage forms only elongated deposits in the bottom of the valleys, often of insufficient dimension to characterize pixels. The es1 stage is mainly present on elevated and slightly sloping surfaces where erosion processes are minimal and the soils conserve the A, B, and C sequence of horizons. On the shoulder of the slope, erosion will be maximum and the C horizon (arkose) is exposed, thus defining an es3a erosion stage. On the back slopes, the erosion processes frequently expose the Bt horizon, therefore, representing the es2b and es2c erosion stages. Within the southern regions, where fine textures and materials rich in calcium carbonate are the most widespread, es2a and es3b erosion stages as well as am2 accumulation stage are the dominant classes. The es2a and es3b stages were encountered on the back slopes. The es3c stage

TABLE V
DESCRIPTION OF FIELD VALIDATION CRITERIA FOR THE SEAS

SEAS		Code	Field validation criteria for samples
Accumulation stage: deposits in footslope and toeslope positions		am1	Type of structure (surface and subsurface horizons): subangular blocky or single grain; grade of structure: weak or structureless; consistence (dry): soft or loose; Munsell color(dry): Hue 10YR or 2.5Yand value 6 or lighter and Chroma 3 or weaker.
		am2	Type of structure (surface and subsurface horizons): angular blocky or platy; grade of structure moderate; consistence (dry): hard; and Munsell color(dry): Hue 10YR and value 5 or darker and Chroma 2 or weaker .
Erosion stages	Stage 1: slightly eroded soil.	es1	Munsell color at different depths; surface: dominant Hue 10YR or more yellow; between 20 and 50 cm depth: Hue 7.5YR or more red with a hard or very hard consistence (dry); and 50–60 cm: a Munsell color (dry): Hue 10YR or 2.5Y and value 6 or lighter and Chroma 3 or weaker.
	Stage 2: moderately eroded soil.	es2a	Type of structure (surface horizon): angular blocky; grade of structure: moderate; consistence (dry): moderately hard or hard; Munsell color (dry): Hue 10YR or yellower and value 5 or darker .
		es2b	Type of structure (surface horizon): angular blocky; grade of structure: strong; consistence (dry): hard or very hard; Munsell color (dry): Hue 10YR or 2.5Y and value 5 or darker. 50–60 cm, subangular or massive structure; moderately hard consistence (dry) and a Munsell color (dry): value 6 or lighter and Chroma 3 or weaker .
		es2c	Type of structure (surface horizon): angular blocky; grade of structure: strong; consistence (dry): hard or very hard; Munsell color (dry): Hue 7.5YR or 5YR and value 5 or darker and Chroma 4 or stronger. 50–60 cm, subangular or massive structure; moderately hard consistence (dry) and a Munsell color (dry): value 6 or lighter and Chroma 3 or weaker.
	Stage 3: strongly eroded soil.	es3a	Stoniness (surface horizon) >15%; type of structure: angular blocky; consistence (dry): moderately hard or harder; Munsell color (dry): Hue 10YR or 2.5Y and value 6 or lighter and Chroma 3 or weaker .
		es3b	Stoniness (surface horizon) <15% and positive reaction to HCl (weak or strong effervescence).
		es3c	Stoniness (surface horizon) >15%, and positive reaction to HCl (strong effervescence).

is characteristic of the shoulders of the slopes, where erosion is very active, exposing the altered limestone horizons often as scattered fragments of rocks as a result of plowing. Accumulation of sandy-textured material (am1) locally characterizes some toeslopes; am2 stage, in this southern region, has a significant importance as they are widely represented in small valley bottoms and especially in the alluvial plains and terraces.

Regarding only the bare soil surfaces (see Table IV), the soil erosion stages (es3) related to strongly eroded soils represent 28.6%. Moderately eroded soils, represented by the es2 stage, occupy 25.0%. Slightly eroded soils (es1) represent 6.3%. These results demonstrate the importance of the erosion processes in the studied region. However, the eroded soil material is transported to the accumulation stage that represents 40.1% of the bare soil surface. The relative importance of the different classes of SEAS suggests certain equilibrium of erosion and accumulation in the context of the study region.

E. Validation and Accuracy Assessment of the Spatial Distribution of the SEAS

The validation of the results obtained with the hyperspectral data was done according to the set of criteria based on the assessment, under field conditions, of soil properties related to the different SEAS (see Table V). This assessment was an efficient way to identify the A, B, or C horizons exposed at the surface according to the soil models that were established for this work (see Fig. 4). Thus, this soil assessment was used to determine the SEAS of a separate set of ground truth points that were then included for validating the SVM classification result. A set of 20 validation points for the npv throughout the region was obtained from field observations and orthoimages.

A confusion matrix (see Table VI) was established with 217 validation points. The overall accuracy obtained for the data was 77% with a kappa coefficient of 0.74. These values are considered as having a relatively high accuracy (given the difficulty of the classification scenario) and have been obtained for the different SEAS within a complex mosaic of erosion and accumulation processes that occur throughout the study region.

The producer's accuracy for individual classes of the SEAS varies between 68.2% (es2c) and 84% (am1) showing how well a certain region is classified. The user's accuracy varies between 61% (es2b) and 90% (es3c) indicating the probability that the pixel classified on the image actually represents that class. In general, the stages are well classified. Most confusions

TABLE VI
CONFUSION MATRIX OF THE SVM CLASSIFICATION SHOWING THE INDIVIDUAL CLASS ACCURACY AS WELL AS PRODUCER'S AND USER'S ACCURACY

	Ground truth validation sites (%)										Total	Prod. acc.	User acc.
Classification	am1	am2	es1	es2a	es2b	es2c	es3a	es3b	es3c	npv	(%)	(%)	(%)
am1	84.0	14.3	0	4.6	8.7	0	0	0	0	5.0	12.9	84.0	75.0
am2	8.0	71.4	0	4.6	0	0	0	0	0	0	8.3	71.4	83.3
es1	0	0	70.0	0.0	13.0	18.2	5.0	0	0	0	10.1	70.0	63.6
es2a	8.0	9.5	5.0	72.7	0	0	0	13.6	0	0	11.1	72.7	66.7
es2b	0	4.8	10.0	9.1	73.9	13.6	15.0	0	0	0	12.9	73.9	60.7
es2c	0	0	10.0	0	4.4	68.2	0	0	0	0	8.3	68.2	83.3
es3a	0	0	5.0	0	0	0	75.0	4.6	0	0	7.8	75.0	88.2
es3b	0	0	0	9.1	0	0	0	77.3	18.2	0	10.6	77.3	73.9
es3c	0	0	0	0	0	0	5.0	4.6	81.8	0	9.2	81.8	90.0
npv	0	0	0	0	0	0	0	0	0	95.0	9.2	95.0	100.0
Total (%)	100.0	100.0	100.0	100.0	100.0	100.0	100.0	100.0	100.0	100.0	100.0		

are easily explained and are logical from the point of view of the complex mosaic of soil surface properties.

Regarding the stages am1 and am2, they are, in general, well classified. However, there is some confusion between the two classes, probably derived from an overlapping of depositional processes in the valley bottoms. This also occurs with es2a due to the coarse sandy arkose material that these classes contain and the weakly developed Bw horizon in es2a. The am2 also has a slight confusion with es2b due to the clay content that both classes may contain. The es1 is mainly confused with the classes also containing clay minerals and iron oxide contents (es2b, es3b, and es3a). The small percentage of confusion that is encountered with the es2 classes is in most cases explainable. In this case, es2b has some confusion with am1, es1, and es2c classes. The es3 classes are best classified and any confusion that does occur is easily explained due to their dominant soil properties such as clay minerals, iron oxides, and $CaCO_3$ content. Although es3c has a high $CaCO_3$ content, there is a slight confusion with es3b which may reach significant $CaCO_3$ content.

The npv class could be determined with a high accuracy and differentiated well from all the other classes due to the well differentiated spectral characteristics. There is slight confusion when the percentage of dry residue becomes low and the underlying soil surface becomes more apparent.

V. CONCLUSION

The integrated method outlined in this work is based on field and laboratory data together with spectral information obtained from the hyperspectral imagery data and it has been possible to identify and map SEAS within a Mediterranean rainfed cultivated region.

The incorporation of site-specific data provided an important basis for successful classification. Improved identification and characterization of the individual SEAS were achieved by the use of the spectral library (MEDSES) that was compiled together with soil analyses, field observation, and ancillary data. This was fundamental for the selection of endmembers used as training sites for the SVM classifier.

A qualitative procedure based on the assumption that physico-chemical and morphological properties related to the different horizons that constitute the main soils present at the terrain surface as a consequence of soil erosion induced by tillage was key to assess the SEAS. As a result, three main erosion stages for slightly, moderately, and strongly eroded soils and an accumulation stage were established. This was especially important for the characterization of reference samples that were needed for the interpretation of the spectral and spatial variation observed in the hyperspectral imagery and was also crucial for validation purposes of the classification result.

The method outlined in this paper has proven successful in determining the spatial variation of soil surface properties even though these variations are often associated with subtle changes in the clay, iron oxide, $CaCO_3$, and sand content. Defining pure endmembers of the different stages is based on several different soil properties and depending on the stage may represent a combination of these properties.

The main soils that characterize the study region are *Haploxeralfs*, *Haploxerept*s, and *Calcixerepts* and these are widely represented soils within Mediterranean environments. Therefore, the proposed method is potentially applicable to other Mediterranean regions with rainfed cultivation.

ACKNOWLEDGMENT

The authors would like to thank the Airborne Research and Survey Facility of the Natural Environment Research Council (ARSF NERC) flight operators and the ARSF Data Analysis Node Remote Sensing Group for the efficient management of the hyperspectral AISA and LIDAR data acquisition and preprocessing, respectively. They are very grateful to F. Pustlauck for participating in the field work operating a spectroradiometer and to Dr. K. Segl for all his recommendations for the hyperspectral data preprocessing and the development of additional programming routines. They would also like to thank Dr. H. Feilhauer for his recommendations of using the SVM classifier in the R environment, and Dr. R. Millán, C. Rico, E. Rodríguez, P. Gil, C. Cabrales, F. Expósito, J. Rodríguez, J. Carlos Díaz, and R. Saldaña for the logistical support in the field and technical laboratory work.

REFERENCES

[1] E. Ben-Dor *et al.*, "Using imaging spectroscopy to study soil properties," *Remote Sens. Environ.*, vol. 113, pp. S38–S55, 2009.

[2] P. Lagacherie, F. Baret, J. B. Feret, J. M. Netto, and J. M. Robbez-Masson, "Estimation of soil clay and calcium carbonate using laboratory, field and airborne hyperspectral measurements," *Remote Sens. Environ.*, vol. 112, pp. 825–835, 2008.

[3] S. Chabrillat, A. F. H. Goetz, L. Krosley, and H. W. Olsen, "Use of hyperspectral images in the identification and mapping of expansive clay soils and the role of spatial resolution," *Remote Sens. Environ.*, vol. 82, pp. 431–445, 2002.

[4] M. R. Nanni and J. A. M. Demattê, "Spectral reflectance methodology in comparison to traditional soil analysis," *Soil Sci. Soc. Amer. J.*, vol. 70, pp. 393–407, 2006.

[5] A. Stevens, M. Nocita, G. Tóth, L. Montanarella, and B. van Wesemael, "Prediction of soil organic carbon at the European scale by visible and near infrared reflectance spectroscopy," *PLoS ONE*, vol. 8, no. 6, pp. 1–13, 2013.

[6] H. Bartholomeus, G. Epema, and M. Schaepman, "Determining iron content in Mediterranean soils in partly vegetated regions, using spectral reflectance and imaging spectroscopy," *Int. J. Appl. Earth Observ. Geoinf.*, vol. 9, pp. 194–203, 2007.

[7] C. Gómez, P. Lagacherie, and G. Coulouma, "Regional predictions of eight common soil properties and their spatial structures from hyperspectral Vis–NIR data," *Geoderma*, vol. 189–190, pp. 176–185, 2012.

[8] F. Previtali, "Pedoenvironments of the Mediterranean countries: Resources and threats," in *Soil Security for Ecosystem Management*, S. Kapur and S. Erşahin, Eds. New York, NY, USA: Springer, 2014, ch. 4, pp. 61–82.

[9] C. Kosmas *et al.*, "The effect of land use on runoff and soil erosion rates under Mediterranean conditions," *Catena*, vol. 29, pp. 45–59, 1997.

[10] J. M. García-Ruiz, "The effects of land uses on soil erosion in Spain: A review," *Catena*, vol. 81, pp. 1–11, 2010.

[11] M. de Luis, J. C. Gonzalez-Hidalgo, and L. A. Longares, "Is rainfall erosivity increasing in the Mediterranean Iberian Peninsula?" *Land Degrad. Dev.*, vol. 21, pp. 139–144, 2010.

[12] S. De Alba, "Modeling the effects of complex topography and patterns of tillage on soil translocation by tillage with mouldboard plough," *J. Soil Water Conserv.*, vol. 56, pp. 335–345, 2001.

[13] D. Gibbon, "Rainfed farming systems in the Mediterranean region," *Plant Soil*, vol. 58, pp. 59–80, 1981.

[14] M. J. Lindstrom, W. W. Nelson, and T. E. Schumacher, "Quantifying tillage erosion rates due to moldboard plowing," *Soil Tillage Res.*, vol. 24, pp. 243–255, 1992.

[15] C. Ortega, *Estudio Agrobiológico de la Provincia de Toledo*. Consejo Superior de Investigaciones Científicas C.S.I.C.—Instituto Provincial de Investigaciones y Estudios Toledanos, Toledo, Spain, 1984, Mapa de suelos E. 1:200.000.

[16] G. B. M. Heuvelink and R. Webster, "Modelling soil variation: Past, present, and future," *Geoderma*, vol. 100, pp. 269–301, 2001.

[17] E. Ben-Dor *et al.*, "Quantitative mapping of the soil rubification process on sand dunes using an airborne hyperspectral sensor," *Geoderma*, vol. 131, pp. 1–21, 2006.

[18] T. Schmid, M. Koch, and J. Gumuzzio, "Application of hyperspectral imagery to map soil salinity," in *Remote Sensing of Soil Salinization: Impact and Land Management*, G. Metternicht and A. Zinck, Eds. Boca Raton, FL, USA: CRC Press/Taylor and Francis, 2008, ch. 7, pp. 113–139.

[19] A. Vrieling, S. M. de Jong, G. Sterk, and S. C. Rodrigues, "Timing of erosion and satellite data: A multi-resolution approach to soil erosion risk mapping," *Int. J. Appl. Earth Observ. Geoinf.*, vol. 10, no. 3, pp. 267–281, 2008.

[20] C. Corbane, D. Raclot, F. Jacob, J. Albergel, and P. Andrieux, "Remote sensing of soil surface characteristics from a multiscale classification approach," *Catena*, vol. 75, pp. 308–318, 2008.

[21] J. Hill and B. Schütt, "Mapping complex patterns of erosion and stability in dry Mediterranean ecosystems," *Remote Sens. Environ.*, vol. 74, pp. 557–569, 2000.

[22] T. Schmid, M. Koch, J. Gumuzzio, and I. Medel, "Field and imaging spectroscopy to determine soil degradation stages in semi-arid terrestrial ecosystems," in *New Quality in Environmental Studies, Imaging Spectroscopy*, B. Zagajewski and M. Sobczak, Eds. Warsaw, Poland: Wydawnictwa Przemyslowe WEMA Sp., 2005, pp. 175–183.

[23] R. Mathieu, B. Cervelle, D. Rémy, and M. Pouget, "Field-based and spectral indicators for soil erosion mapping in semi-arid Mediterranean environments (Coastal Cordillera of central Chile)," *Earth Surf. Process. Landforms*, vol. 32, pp. 13–31, 2007.

[24] N. Brunel, F. Meza, R. Ros, and F. Santibáñez, "Effects of topsoil loss on wheat productivity in dryland zones of Chile," *J. Soil Sci. Plant Nutr.*, vol. 11, no. 4, pp. 129–137, 2011.

[25] S. Jagadamma, R. Lal, and B. K. Rimal, "Effects of topsoil depth and soil amendments on corn yield and properties of two Alfisols in central Ohio," *J. Soil Water Conserv.*, vol. 64, no. 1, pp. 70–80, 2009.

[26] Ministerio de Agricultura, Alimentación y Medio Ambiente—MAGRAMA, Servicios, Cartografía y SIG. SIGA-Sistema de Información Geográfica de Datos Agrarios, Madrid, Spain, 2014.

[27] A. Martín-Serrano, J. A. Díaz de Neira, and F. L. López-Olmedo, *Mapa Geológico de España, escala 1:50.000. Villaluenga de la Sagra 604 (18-24)*, Instituto Geológico y Minero de España, Madrid, Spain, 1999.

[28] Soil Survey Staff, *Keys to Soil Taxonomy*, 12th ed.Washington, DC, USA: USDA-Natural Resources Conservation Service, 2014.

[29] Ministerio de Agricultura. (2014). *Alimentación y Medio Ambiente—MAGRAMA, Metadatos* [Online]. Available: http://www.magrama.gob.es/es/cartografia-y-sig/ide/descargas/default.aspx

[30] Instituto Geológico y Minero de España—IGME. (2014). *Cartografía Geológica* [Online]. Available: http://mapas.igme.es/Servicios/default.aspx

[31] Instituto Geográfico Nacional—IGN. (2014). *Topografía y Orthoimagenes* [Online]. Available: http://www.ign.es/ign/layout/faimsatinicio.do

[32] Ministerio de Agricultura. (2014). *Alimentación y Medio Ambiente—MAGRAMA, Visor del SIGPAC* [Online]. Available: http://sigpac.mapa.es/fega/visor/mber

[33] P. J. Schoeneberger, D. A. Wysocki, E. C. Benham, and Soil Survey Staff, *Field Book for Describing and Sampling Soils, Version 3.0*. Lincoln, NE, USA: Natural Resources Conservation Service, National Soil Survey Center, 2012.

[34] G. Govers, K. Vandaele, P. J. J. Desmet, J. Poesen, and K. Bunte, "The role of tillage in soil redistribution on hillslopes," *Eur. J. Soil Sci.*, vol. 45, pp. 469–478, 1994.

[35] S. De Alba, M. Lindstrom, T. E. Schumacher, and D. D. Malo, "Soil landscape evolution due to soil redistribution by tillage: A new conceptual model of soil catena evolution in agricultural landscapes," *Catena*, vol. 58, pp. 77–100, 2004.

[36] C. M. Rostagno and G. Degorgue, "Desert pavements as indicators of soil erosion on aridic soils in north-east Patagonia (Argentina)," *Geomorphology*, vol. 134, pp. 224–231, 2011.

[37] C. O. Justice and J. G. Townshend, "Integrating ground data with remote sensing," in *Terrain Analysis and Remote Sensing*, J. G. Townshend, Ed. London, U.K.: G. Allen, 1981.

[38] S. Schmidtlein, P. Zimmermann, R. Schüpferling, and C. Weiß, "Mapping the floristic continuum: Ordination space position estimated from imaging spectroscopy," *J. Veg. Sci.*, vol. 18, pp. 131–140, 2007.

[39] W. H. Press, S. A. Teukolsky, W. T. Vetterling, and B. P. Flannery, *Numerical Recipes in C: The Art of Scientific Computing*. Cambridge, U.K.: Cambridge Univ. Press, 1992.

[40] Exelis Visual Information Solutions, Inc., *The Environment for Visualizing Images (ENVI) Version 5.2*, Boulder, CO, USA, 2014.

[41] R. Burt, "Soil survey field and laboratory methods manual," Nat. Soil Survey Center, Nat. Resour. Conserv. Service, U.S. Dept. Agric., Lincoln, NE, USA, Soil Survey Investigations Rep. No. 51 Version 1.0, 2009.

[42] Environmental Systems Research Institute Inc., *ArcGis 9.3*. Redlands, CA, USA: Environmental Systems Research Institute Inc., 2011.

[43] T. Wasklewicz, D. M. Staley, K. Reavis, and T. Oguchi, "3.6 Digital terrain modelling," *Treatise Geomorphol.*, vol. 3, pp. 130–161, 2013.

[44] D. R. Streutker and N. F. Glenn, "LiDAR measurement of sagebrush steppe vegetation heights," *Remote Sens. Environ.*, vol. 102, no. 1–2, pp. 135–145, 2006.

[45] D. Chen, C. T. Lu, Y. Kou, and F. Chen, "On detecting spatial outliers," *GeoInformatica*, vol. 12, no. 4, pp. 455–475, 2008.

[46] R. Richter, "Atmospheric/topographic correction for wide FOV airborne imagery: Model ATCOR4 (version 6.2.0)," DLR, Wessling, Germany, Rep. DLR-IB 552-05/99, 2012.

[47] A. A. Green, M. Berman, P. Switzer, and M. D. Craig, "A transformation for ordering multispectral data in terms of image quality with implications for noise removal," *IEEE Trans. Geosci. Remote Sens.*, vol. 26, no. 1, pp. 65–74, Jan. 1988.

[48] J. W. Boardman, F. A. Kruse, and R. O. Green, "Mapping target signatures via partial unmixing of AVIRIS data," in *Proc. Summaries 5th JPL Airborne Earth Sci. Workshop*, 1995, vol. 95, pp. 23–26.

[49] J. W. Boardman, "Automated spectral unmixing of AVIRIS data using convex geometry concepts," in *Proc. Summaries 4th JPL Airborne Geosci. Workshop*, 1993, vol. 1, pp. 11–14.

[50] G. M. Foody and A. Mathur, "A relative evaluation of multiclass image classification by support vector machines," *IEEE Trans. Geosci. Remote Sens.*, vol. 42, no. 6, pp. 1336–1343, Jun. 2004.

[51] G. Foody and A. Mathur, "Toward intelligent training of supervised image classifications: Directing training data acquisition for SVM classification," *Remote Sens. Environ.*, vol. 93, no. 1, pp. 107–117, 2004.
[52] F. Melgani and L. Bruzzone, "Classification of hyperspectral remote sensing images with support vector machines," *IEEE Trans. Geosci. Remote Sens.*, vol. 42, no. 8, pp. 1778–1790, Aug. 2004.
[53] G. Foody and A. Mathur, "The use of small training sets containing mixed pixels for accurate hard image classification: Training on mixed spectral responses for classification by a SVM," *Remote Sens. Environ.*, vol. 103, no. 2, pp. 179–189, 2006.
[54] D. Meyer *et al.* (2014). *e1071: Misc Functions of the Department of Statistics (e1071), TU Wien, Version 1.6-4* [Online]. Available: http://cran.r-project.org/web/packages/e1071/e1071.pdf
[55] R. J. Hijmans *et al.* (2015). *Geographic Data Analysis and Modeling, Version 2.3-40* [Online]. Available: http://cran.r-project.org/web/packages/raster/raster.pdf
[56] R. Bivand *et al.* (2015). *Bindings for the Geospatial Data Abstraction Library, Version 1.0-4* [Online]. Available: http://cran.r-project.org/web/packages/rgdal/rgdal.pdf
[57] R Development Core Team. (2005). R: A language and environment for statistical computing, R Foundation for Statistical Computing, Vienna, Austria [Online]. Available: http://www.R-project.org/
[58] P. L. Nagler, C. S. T. Daugherty, and S. N. Goward, "Plant litter and soil reflectance," *Remote Sens. Environ.*, vol. 71, pp. 207–215, 2000.
[59] S. Chabrillat *et al.*, "HYSOMA: An easy-to-use software interface for soil mapping applications of hyperspectral imagery," in *Proc. 7th EARSeL SIG Imaging Spectrosc. Workshop*, Edinburgh, U.K., Apr. 11–13, 2011, pp. 1–7.
[60] C. W. Hsu, C. C. Chang, and C. J. Lin. (2010). *A Practical Guide to Support Vector Classification*, Dept. Comput. Sci., Nat. Taiwan Univ., Taipei, Taiwan [Online]. Available: http://www.csie.ntu.edu.tw/~cjlin/libsvm
[61] R. G. Congalton, "A review of assessing the accuracy of classifications of remotely sensed data," *Remote Sens. Environ.*, vol. 37, pp. 35–46, 1991.
[62] A. Palacios-Orueta and S. L. Ustin, "Remote sensing of soil properties in the Santa Monica mountains. I. Spectral analysis," *Remote Sens. Environ.*, vol. 65, no. 2, pp. 170–183, 1998.
[63] K. D. Shepherd and M. G. Walsh, "Development of reflectance spectral libraries for characterization of soil properties," *Soil Sci. Soc. Amer. J.*, vol. 66, no. 3, pp. 988–998, 2002.

Thomas Schmid (M'07) received the M.Sc. degree in geography from the University of Zürich, Zürich, Switzerland, and the Ph.D. degree in science from the Autonomous University of Madrid, Madrid, Spain, in 1993 and 2004, respectively.

Since 1994, he has been a Researcher with the Department of Environment, Research Centre for Energy, Environment and Technology (CIEMAT), Madrid, Spain. He integrates hyper- and multispectral optical data and polarimetric SAR data to characterize and monitor the exploitation of soil resources and the conservation of natural ecosystems in semiarid regions and within ice-free regions of Antarctica. His research interests include soil erosion and periglacial processes, wetland degradation and heavy metal contamination, and the application of remote sensing and GIS technologies.

Manuel Rodríguez-Rastrero received the M.Sc. degree in biology from the Autonomous University of Madrid, Madrid, Spain, 1990.

Since 2010, he has been with the Department of Environment, Research Centre for Energy, Environment and Technology (CIEMAT), Madrid, Spain, as a Graduate Degree Researcher. He is a Team Member of research projects related to soil degradation, pollution and remediation, and evaluation of crop residues. His research interests include soil mapping and soil assessment projects and soil studies applied to environmental impact assessment and land restoration.

Paula Escribano received the degree in biological science from the Autonomous University of Madrid, Madrid, Spain, in 2007, the M.Sc. degree in geoinformation science from the Wageningen University, Wageningen, The Netherlands, and the Ph.D. degree in science from the University of Almería, Almería, Spain, in 2000, 2002 and 2009, respectively.

She is currently working as a Researcher with the Spanish Research Council, Madrid, Spain. Her research interests include the use of hyperspectral and multitemporal data for studying ecosystem dynamics and land degradation, CO_2 fluxes, and arid environments.

Alicia Palacios-Orueta received the agricultural engineering degree from the Technical University of Madrid, Madrid, Spain, in 1990, and the M.Sc. and Ph.D. degrees in soil science from the University of California, Davis, Davis, CA, USA, in 1994 and 1997, respectively.

Since 2003, she has been with the Department of Systems and Natural Resources, Technical University of Madrid, Madrid, Spain, as a Professor. Her research interests include the development of vegetation indexes and the analysis of remote sensing time series with application to the natural and agricultural ecosystems.

Eyal Ben-Dor received the M.Sc. and Ph.D. degrees in soil science from the Faculty of Agriculture, Hebrew University of Jerusalem, Israel, in 1986 and 1992, respectively.

Currently, he is serving as the Chair of the Geography Department, Tel Aviv University, Tel Aviv, Israel, and the Head of the Remote Sensing Laboratory (RSL), Tel Aviv University. He has more than 22 years experience in remote sensing of the Earth with a special emphasis on the hyperspectral remote sensing (HSR), soil spectroscopy (passive and active), and environmental issues. His research interests include monitoring the Earth from space and air as well as on developing innovative tools to monitor soils and minerals from all domains.

Antonio Plaza (M'05–SM'07–F'15) is an Associate Professor (with accreditation for Full Professor) with the Department of Technology of Computers and Communications, University of Extremadura, Cáceres, Spain, where he is the Head of the Hyperspectral Computing Laboratory (HyperComp). He has authored more than 500 publications, including more than 150 journal papers. His research interests include hyperspectral data processing and parallel computing of remote sensing data.

Dr. Plaza was the recipient of the recognition of Best Reviewers of the IEEE GEOSCIENCE AND REMOTE SENSING LETTERS, in 2009, and the recipient of the recognition of Best Reviewers of the IEEE TRANSACTIONS ON GEOSCIENCE AND REMOTE SENSING, in 2010, He is a recipient of the 2013 Best Paper Award of the JSTARS journal and is currently serving as President of the Spanish Chapter of the Geoscience and Remote Sensing Society. He is currently serving as the Editor-in-Chief of the IEEE TRANSACTIONS ON GEOSCIENCE AND REMOTE SENSING JOURNAL. Additional information: http://www.umbc.edu/rssipl/people/aplaza

Robert Milewski received the M.Sc. degree in geography from the Free University of Berlin, Berlin, Germany, in 2013. Since 2013, he has been pursuing the Ph.D. degree in remote sensing from the Helmholtz Centre Potsdam—German Research Centre for Geosciences (GFZ), Potsdam, Germany.

His research interests include remote sensing of soils and dry lands as well as geomorphology and soil erosion processes, paleoenvironmental reconstruction, and the investigation of landscape changes.

Margarita Huesca received the forestry engineering degree from the Technical University of Madrid, Madrid, Spain, in 2007, the M.Sc. degree in geoinformation science from Wageningen University, Wageningen, The Netherlands, in 2007, and the Ph.D. degree in agricultural enginnering from the Technical University of Madrid, in 2013.

She is a Postdoctoral Researcher with the Department of Land Air and Water Resources, Center for Spatial Technologies and Remote Sensing (CSTARS), University of California Davis, Davis, CA, USA. Her research interests include statistical time series analysis for quantifying and monitoring ecological processes, such as forest fires, phenological dynamics, evapotranspiration in Mediterranean regions, and vegetation structure assessment with imaging spectroscopy data.

Ashley Bracken received the B.Sc. and M.Sc. degrees in geography from the University of Lethbridge, AB, Canada, in 2010 and 2014, respectively.

She is currently a Research Assistant with the Alberta Terrestrial Imaging Centre (ATIC), University of Lethbridge. Her research interests include hyperspectral image processing and application for soil erosion monitoring and land reclamation purposes.

Víctor Cicuéndez received the degrees in forestry engineering and environmental sciences and the M.Sc. degree in sustainable agroforestry engineering from the Technical University of Madrid, Madrid, Spain (UPM), in 2011 and 2012, respectively. Since 2013, he has been pursuing the Ph.D. degree from the UPM.

His research interests include ecology and ecological modeling, remote sensing, the study of CO_2 and other fluxes in ecosystems, and the application of statistical time series analysis to remote sensing and environmental data.

Marta Pelayo received the M.Sc. degree in geology and the Ph.D. degree in geology from the Complutense University of Madrid, Madrid, Spain, in 1988 and 2014.

Since 1990, she has been a Researcher with the Department of Environment, Research Centre for Energy, Environment and Technology (CIEMAT), Madrid, Spain. Her research interests include soil erosion, mineralogy and geochemistry of clay minerals, and alteration processes and characterization of heavy metal contaminated soils, as well as CO_2, water, and rock interaction processes.

Sabine Chabrillat received the B.Sc. degree in physics and Ph.D. degree in geophysics and space technics from the University of Toulouse III, Toulouse, France, in 1990 and 1995, respectively. She did her postdoctoral studies at CSES/University of Colorado, Boulder, CO, USA.

Since 2001, she has been a Senior Researcher with the GFZ German Research Centre for Geosciences, Potsdam, Germany. Her research interests include developments in optical and thermal imaging spectroscopy for geosciences and environmental applications, quantitative soil spectroscopy, laboratory—proximal—Earth observation drylands sensing, and soil erosion and degradation processes.